Dynamics of scattering on a classical two-dimensional artificial atom

H. Peelaers,[1,*] B. Partoens,[1,†] D. V. Tatyanenko,[1,2,‡] and F. M. Peeters[1,§]
[1]*Departement Fysica, Universiteit Antwerpen, Groenenborgerlaan 171, B-2020 Antwerpen, Belgium*
[2]*Laboratorium voor Vaste-Stoffysica en Magnetisme, Katholieke Universiteit Leuven, 3001 Leuven, Belgium*
(Received 13 July 2006; revised manuscript received 4 December 2006; published 13 March 2007)

A classical two-dimensional (2D) model for an artificial atom is used to make a numerical "exact" study of elastic and nonelastic scattering. Interesting differences in the scattering angle distribution between this model and the well-known Rutherford scattering are found in the small energy and/or small impact parameter scattering regime. For scattering off a classical 2D hydrogen atom different phenomena such as ionization, exchange of particles, and inelastic scattering can occur. A scattering regime diagram is constructed as function of the impact parameter (b) and the initial velocity (v) of the incoming particle. In a small regime of the (b,v) space the system exhibits chaos, which is studied in more detail. Analytic expressions for the scattering angle are given in the high impact parameter asymptotic limit.

DOI: 10.1103/PhysRevE.75.036606 PACS number(s): 45.05.+x, 45.50.−j

I. INTRODUCTION

The gravitational three-body problem is the simplest nontrivial three-body system. In 1890 Poincaré [1] proved that this problem is nonintegrable and that closed form solutions are very rare. This was the beginning of the study of nonlinear dynamics; but even at this moment not much is known about the dynamics of the three-body problem, due to its large dimensionality, while a good knowledge of it is necessary to study the dynamical properties of the solar system and its long-term stability (see [2] for an overview on this subject).

Related systems are those made up of charged particles. Such systems occur naturally in the study of atoms. Mostly this problem is studied quantum mechanically, which is a very difficult task, in particular if one is interested in the dynamics of it. To gain a better insight in to these solutions, the equivalent classical problem is studied in this paper, where we will restrict ourselves for convenience to two-dimensional (2D) systems. We consider a model system of an atom in two dimensions (2D) so that an easy visualization is possible.

The static properties of 2D classical clusters were studied before. Most studies dealt with classical dots confined by a parabolic potential. However, the static properties of a classical system that is more closely related to real atoms was studied in Ref. [3]. They considered a system consisting of classical charged point particles interacting through a repulsive Coulomb potential but which are held together through the Coulomb potential of a positive charge that is located at a distance d from the 2D plane the particles are moving in. As a function of the strength of the confinement potential, surprising rich physics was observed in Ref. [3] such as structural transitions, spontaneous symmetry breaking, and unbinding of particles, which is absent in parabolic confined dots. Other static phenomena of this model system were studied by Ferreira *et al.* [4] and the linear dynamical properties of this system, namely the normal modes, were investigated in Ref. [5]. In this work, we extend this research to the dynamics of collisions on this system.

The present system is not purely academic but may be realized experimentally. A quantum analog of the present system can be found in semiconductor heterostructures where a two-dimensional electron gas (2DEG) is formed at the interface of two different semiconductors [6]. The 2DEG in a typical high mobility GaAs/AlGaAs heterostructure results from remote doping. These remote dopants also act as scattering centers for the electrons at the interface, limiting their mobility. An electron can also be bound to such a remote dopant resulting in the quantum analog of the system as studied in Sec. III. Another well-known analog is that of electrons above a liquid helium surface, which form a 2DEG (see [7]). These electrons obey the laws of classical mechanics if the density is low. A lateral Coulomb type of confinement can be realized in this system by inserting impurities in the substrate supporting the helium film.

We found that under certain conditions the scattering on this system exhibits chaotic signatures. Chaotic scattering occurs in many areas of physics (see Ref. [8]) and is a topic of current research. In most previous theoretical studies the interaction of an incoming particle with a particular fixed potential or the motion within a specific shaped boundary was studied (e.g., [9,10]). In this paper we extend this research to the case where the potential varies dynamically with the motion of the particles.

This paper is organized as follows. In Sec. II the model system is introduced, the necessary equations are derived, and the method of solution is explained. The method is applied to Rutherford scattering and to the scattering on the classical 2D H^+ ion. Both cases can be solved analytically and serve as a test for our numerical program. In Sec. III we discuss the scattering properties on a classical hydrogen atom and discuss the richness in the dynamics of this system. Our conclusions are summarized in Sec. IV.

*Electronic address: hartwin.peelaers@ua.ac.be
†Electronic address: bart.partoens@ua.ac.be
‡Electronic address: dmitry.tatyanenko@fys.kuleuven.be
§Electronic address: francois.peeters@ua.ac.be

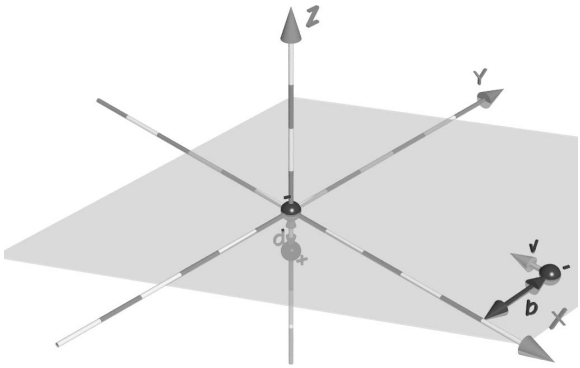

FIG. 1. Schematic view of the model system in the case of one bound particle and one incoming particle characterized by its velocity v and by the impact parameter b.

II. MODEL AND METHOD OF SOLUTION

The model system consists of N bound negatively charged point particles (with charge $-e$) interacting through repulsive Coulomb interactions. The system is held together by the attractive Coulomb interaction to a remote positively charged particle (with charge $+Ze$). The motion of the negative particles is constrained to a 2D plane. The positive particle (the impurity) is fixed at a distance d from the plane and is situated in a medium with dielectric constant ϵ.

The potential energy for our system is given by

$$V = \frac{e^2}{\epsilon_0}\sum_{i=1}^{N}\sum_{j=i+1}^{N}\frac{1}{|\vec{\rho}_i - \vec{\rho}_j|} - \frac{Ze^2}{\epsilon}\sum_{i=1}^{N}\frac{1}{|\vec{\rho}_i + \vec{d}|}, \tag{1}$$

where $\vec{\rho}_i$ is the position of the ith particle in the (x,y)-plane and $\vec{d}=d\vec{e}_z$ is the distance of the positive fixed particle from the 2D plane. The N bound particles are placed in their ground state configuration, which was obtained by performing numerical Monte Carlo simulations followed by a modified Newton technique [11] to realize a higher precision.

To study scattering on this system another negatively charged particle will be taken as an incoming particle. This particle is considered to have an impact parameter b and an initial velocity v at infinity, which characterizes the incoming energy. This system is shown in Fig. 1.

The dynamics of this system are governed by the Newton equations $\vec{F}=m\vec{a}$. If we choose the distance d as our length unit and $e^2/\epsilon_0 d$ as the unit of energy, the following equations of motion are obtained:

$$\begin{pmatrix} \dot{x}_1 \\ \dot{y}_1 \\ \vdots \\ \dot{x}_N \\ \dot{y}_N \\ \dot{v}_{x_1} \\ \dot{v}_{y_1} \\ \vdots \\ \dot{v}_{x_N} \\ \dot{v}_{y_N} \end{pmatrix} = \begin{pmatrix} 0 & I_N \\ M & 0 \end{pmatrix} \begin{pmatrix} x_1 \\ y_1 \\ \vdots \\ x_N \\ y_N \\ v_{x_1} \\ v_{y_1} \\ \vdots \\ v_{x_N} \\ v_{y_N} \end{pmatrix}, \tag{2}$$

where 0 is the $2N\times 2N$ dimensional zero matrix, I_N the $2N\times 2N$ dimensional unit matrix, and M the following $(2N\times 2N)$ matrix:

$$\begin{pmatrix} \sum_{j\neq 1}^{N} A_{1j} - B_1 & 0 & -A_{12} & \cdots & 0 \\ 0 & \sum_{j\neq 1}^{N} A_{1j} - B_1 & 0 & \cdots & -A_{1N} \\ -A_{12} & 0 & \sum_{j\neq 2}^{N} A_{2j} - B_2 & \cdots & 0 \\ \vdots & & & \ddots & \vdots \\ 0 & -A_{1N} & 0 & \cdots & \sum_{j\neq N}^{N} A_{Nj} - B_N \end{pmatrix},$$

with

$$A_{ij} = \frac{1}{[(x_i - x_j)^2 + (y_i - y_j)^2]^{3/2}},$$

$$B_n = \frac{Z^*}{(x_n^2 + y_n^2 + 1)^{3/2}}, \tag{3}$$

where $n=1,\ldots,N$, N is the number of bound particles and $Z^*=Z\epsilon_0/\epsilon$ is the effective charge. This effective charge is taken equal to the number of bound particles N to simulate a

real neutral atom. In this work we will restrict ourselves to systems where N equals 0 or 1.

These equations are solved numerically to obtain the time evolution of the particle motion by a standard adaptive Runge-Kutta algorithm. An important tool to check the precision of the used ordinary differential equation (ODE) solver is the energy, which must be conserved at all times. For example, the difference between its minimum and its maximum value is a measure of the precision of the ODE solver.

A. Application to Rutherford scattering

In standard Rutherford scattering the positive fixed charge is located in the same plane as the incoming particle, i.e., $d=0$. The equations of motion become $v_x=dx/dt$, $v_y=dy/dt$, $dv_x/dt=-Z^*x(x^2+y^2)^{-3/2}$, and $dv_y/dt=-Z^*y(x^2+y^2)^{-3/2}$. Using these equations the trajectories can be calculated and by fitting a straight line through the trajectory after the collision the scattering angle θ can be obtained and the dependence of θ on the initial conditions (b,v) can be investigated.

This scattering angle can also be derived analytically. The derivation for the general case of a central potential can be found in standard textbooks (e.g., see Ref. [12]). The general formula is given by

$$\theta = \pi - 2\int_{r_m}^{\infty} dr \frac{b/r^2}{\left[1-\left(\frac{b}{r}\right)^2 - \frac{V(r)}{T_\infty}\right]^{1/2}}, \tag{4}$$

where r_m is the closest distance between the incoming particle and the scattering center during the trajectory (it corresponds to the largest root of the denominator), T_∞ is the kinetic energy of the incoming particle, and $V(r)$ is the scattering potential. In this particular case it becomes [after inserting the Coulomb potential $V(r)=-1/r$ and using energy conservation]

$$\theta = -2\arctan(1/bv^2). \tag{5}$$

This equation shows that the scattering angle θ depends only on the parameter bv^2.

Both methods give rise to the same Fig. 2. A direct comparison between the theoretical obtained and the simulated results for two initial conditions varying only by a small amount (10^{-11}) show that our ODE solver is capable of this precision.

One sees that in the limit of $bv^2 \to 0$ the incoming particle is backscattered, e.g., $\theta=-\pi+2\sqrt{2}bv^2$. This behavior is illustrated in the inset of Fig. 2, which shows the different trajectories for decreasing bv^2. This behavior is caused by the combined effect that the potential diverges at the origin $[V(r)\sim 1/r]$ and conservation of energy.

B. Application to scattering on a classical 2D hydrogen ion

The well-known results for Rutherford scattering will now be used to compare with scattering on a classical 2D H^+ ion. Therefore we consider the case where $d\neq 0$ (which means placing the positive charge at a certain distance from the plane). The potential becomes, in the earlier defined units,

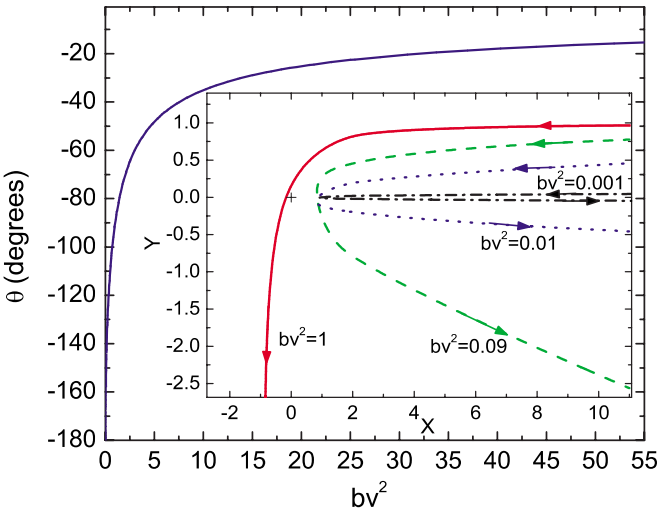

FIG. 2. (Color online) The scattering angle versus bv^2 for Rutherford scattering. The inset shows the trajectories of the incoming particle, moving in a Coulomb potential, as a function of bv^2.

$$V(r) = -\frac{1}{\sqrt{r^2+1}}. \tag{6}$$

Using Eq. (4) we get

$$\theta = \pi - 2\int_{r_m}^{\infty} dr \frac{b/r^2}{\left[1-\left(\frac{b}{r}\right)^2 + \frac{1}{T_\infty\sqrt{r^2+1}}\right]^{1/2}} = \pi - 2I. \tag{7}$$

This integral has no simple analytical solution, but it can be integrated numerically, although the integrand diverges for $r=r_m$. This is better seen when we eliminate b using energy conservation and substituting $u=1/r$, which results into

$$I = \int_0^{1/r_m} \frac{b\,du}{\left[1-r_m^2u^2 - \frac{r_m^2u^2}{T_\infty\sqrt{r_m^2+1}} + \frac{1}{T_\infty\sqrt{u^{-2}+1}}\right]^{1/2}}. \tag{8}$$

The integrand has a square root divergence at its upper limit.

The results are shown in Fig. 3 for different values of b. Note the difference in behavior in the region of small bv^2 between Figs. 2 and 3. To explain this we first look at large impact parameters b. The distance from the particle to the positive charge is then large, so that the interaction strength is small. The particle will be scattered over a very small angle. If the impact parameter becomes smaller, the distance to the positive charge becomes smaller and the interaction stronger, so that the particle will be scattered over a larger angle. In the limit of small b the deflection is small and in the limit of $b=0$ there is no deflection at all. When b is increased, the deflection also increases. This seems contradictory because the interaction strength decreases; but this is compensated by an increase in the interaction time. An addi-

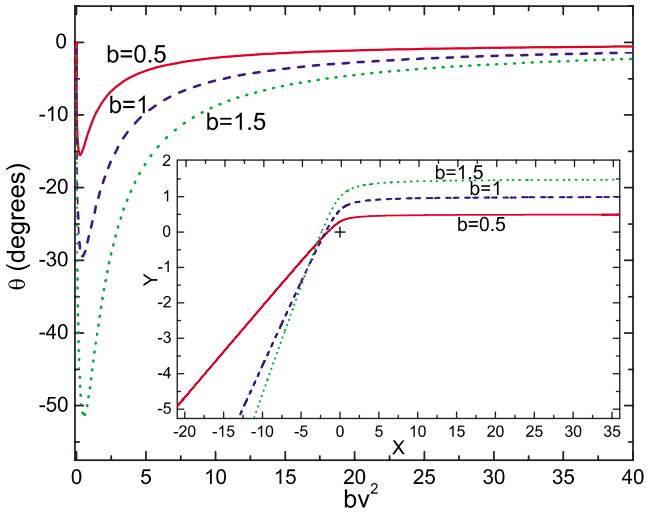

FIG. 3. (Color online) The scattering angle as a function of bv^2 for different b values for the displaced scattering center. The inset illustrates the increase in scattering angle with increasing b values for $v=-1$.

tional effect is that the closer the particle comes to the origin, the faster it will go (because of energy conservation) and hence the smaller the interaction time. This is illustrated in the inset of Fig. 3 where several trajectories are plotted for a fixed velocity, but different b values. There must be a transition from one regime to the other, which explains the local minimum in Fig. 3.

III. SCATTERING ON A CLASSICAL HYDROGEN ATOM

We now add a negative particle to the previous system, which we consider in its minimum energy configuration. In this case this is the origin as can easily be seen from Eq. (1). The effective charge Z^* is again taken equal to 1. This system can be considered as a classical 2D model of a hydrogen atom [19]. We launch a particle on this system. Depending on the initial conditions three different types of collisions can be distinguished.

A. Classification

A first type of collision that can occur is normal scattering. This type of collision occurs when the energy transfer between the incoming particle and the bound particle is smaller than the energy needed to escape from the potential. This energy is given by the difference of the potential when the bound particle is in its original position ($V=-1$) and at infinity ($V=0$). So if the transferred energy is less than 1, the particle remains bound, but the energy it receives will result in elliptic precessing orbits. The incoming particle loses a bit of its energy, so it will slow down, and it will be scattered over a certain angle θ. We will call this type of collision type I and it is illustrated in Fig. 4.

When the transferred energy is larger than 1, the bound particle becomes free. If the remaining energy of the incoming particle becomes negative, this particle becomes trapped and it will move around the origin in precessing elliptic orbits. We will call this kind of collision type II and it is illustrated in Fig. 5. There is an exchange of particles, the bound (free) particle becomes free (bound).

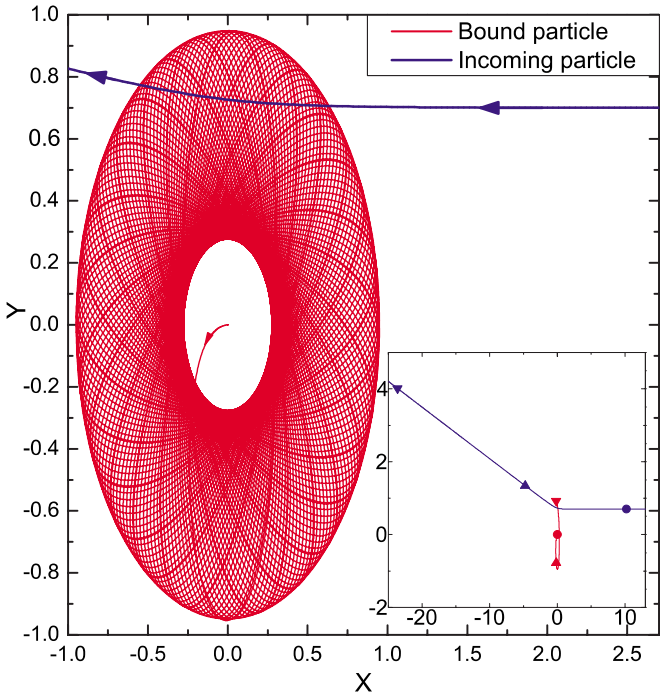

FIG. 4. (Color online) An example of a collision of type I ($b=0.7$ and $v=-3.5$). The inset shows the evolution of the trajectories during the collision. The symbols indicate the positions of the two particles at different times.

The last type, type III, occurs when both particles move freely after the collision. This will be the case if the transferred energy is larger than 1 and the incoming particle has a remaining positive energy. Thus the total energy of the system is positive, so this can only happen when the incoming velocity v is larger then $\sqrt{2}$. This ionization process is shown in Fig. 6.

The scattering process where both particles become bound is not possible when the effective charge Z^* is equal to

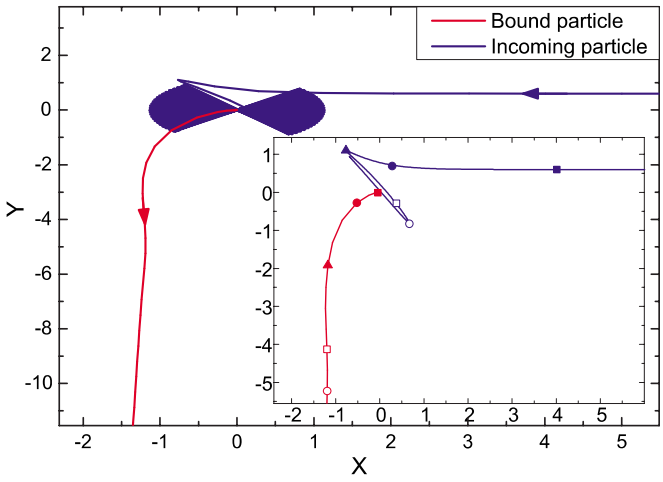

FIG. 5. (Color online) An example of a collision of type II (with $b=0.6$ and $v=-1$). The same convention is used as in Fig. 4.

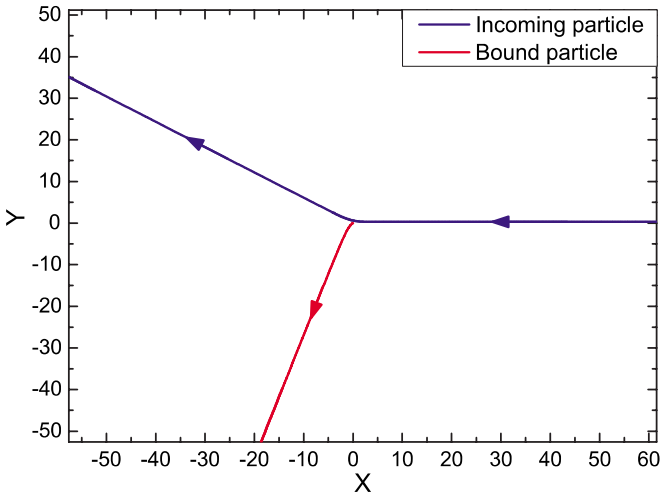

FIG. 6. (Color online) A collision of type III (b=0.3 and v=−3).

1. In the static case the only stable minimum configuration that can be reached is where one of the particles is in the origin and the other is at infinity. Even in the dynamical case it is not possible to have both particles bound because both particles will continually exchange energy and at a certain moment one of the particles will have enough energy to escape from the potential.

Using the amount of transferred energy it is possible to make a distinction between the three types of collision. Figure 7 is an example of a typical energy transfer diagram, for a fixed impact parameter of b=0.3 where ΔE_1 is equal to the energy transferred from the bound particle to the incoming, ΔE_2 the energy transferred from the incoming to the bound particle, and $E_2(\infty)$ is the energy of the incoming particle after the collision (at time $t=\infty$).

Using such energy transfer diagrams a scattering regime diagram is made (see Fig. 8), which shows the occurrence of each type of collision depending on the initial conditions b and v.

The inset shows the same graph, but on a logarithmic scale. The asymptotic boundaries (for small b) are shown as red lines. These asymptotic boundaries are, respectively, v =0.355, $b=2\sqrt{2}v^{-3}$, and $b=\sqrt{2}v^{-1}$.

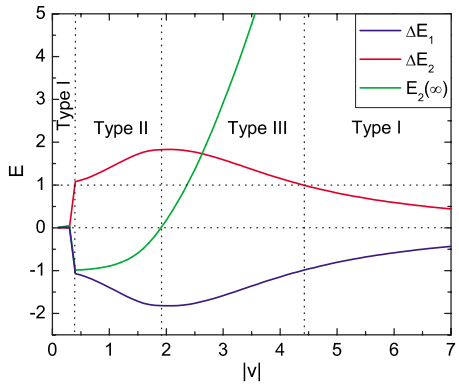

FIG. 7. (Color online) Energy transfer using b=0.3. The three types of collisions are separated by dotted lines.

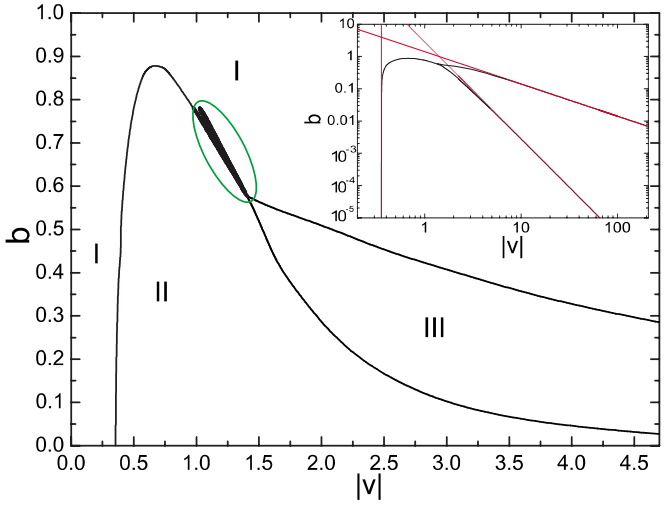

FIG. 8. (Color online) Scattering regime diagram indicating the three different types of collisions as a function of the initial conditions. In the area indicated with an ellipse the type of collision becomes strongly dependent on the initial conditions (see Sec. III B). The inset shows the same graph in log-log scale. Asymptotic boundaries (for small b) are shown by the lines.

B. Chaotic regime

The area indicated in Fig. 8 by the ellipse is special. In this area the collision type changes between type I and type II within small variations of b and/or v. It exhibits chaotic behavior. This can be seen in Fig. 9 which shows a part of this area in more detail. To construct this figure we chose random initial conditions and numerically determined the type of collision which is then represented by a colored point on the figure. The reason to choose random initial conditions instead of a regular grid is that this allows one to see a finer structure with less calculated points. An alternation of the

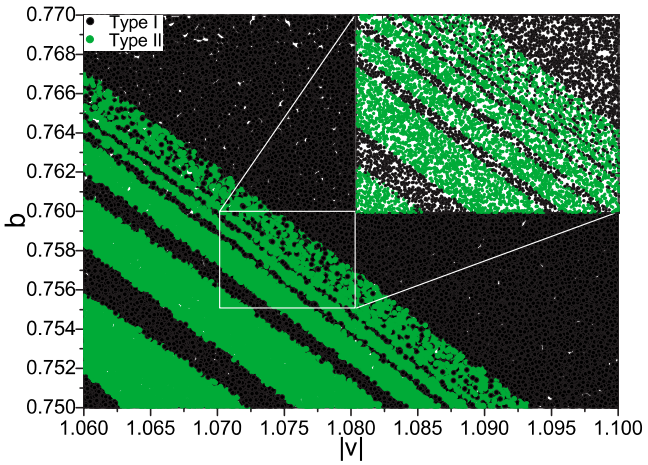

FIG. 9. (Color online) A more detailed view of an area inside the marked ellipse in Fig. 8. The different colors indicate the type of collision (either type I or type II). As can be seen the type changes quickly with the initial conditions. A stripelike pattern can be observed. The inset shows a zoom of the marked rectangular area. The white rectangular area inside the inset indicates the box used for the calculation of the uncertainty dimension.

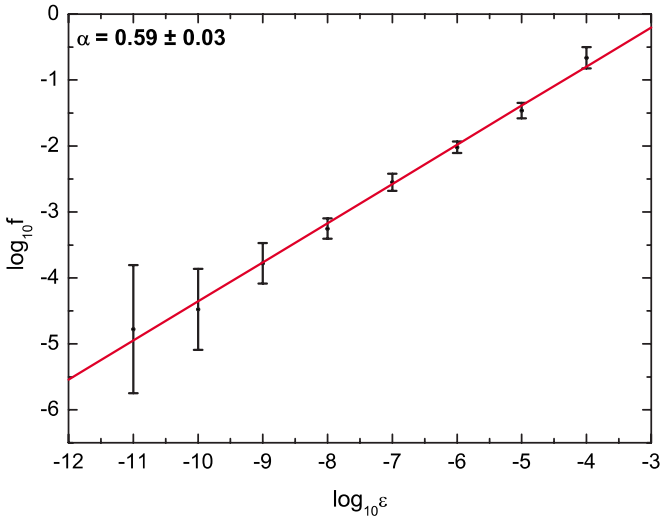

FIG. 10. (Color online) A least-squares fit of $\log_{10} f(\epsilon)$ versus $\log_{10} \epsilon$. The slope α is equal to 0.59±0.03 and consequently the boundary is fractal.

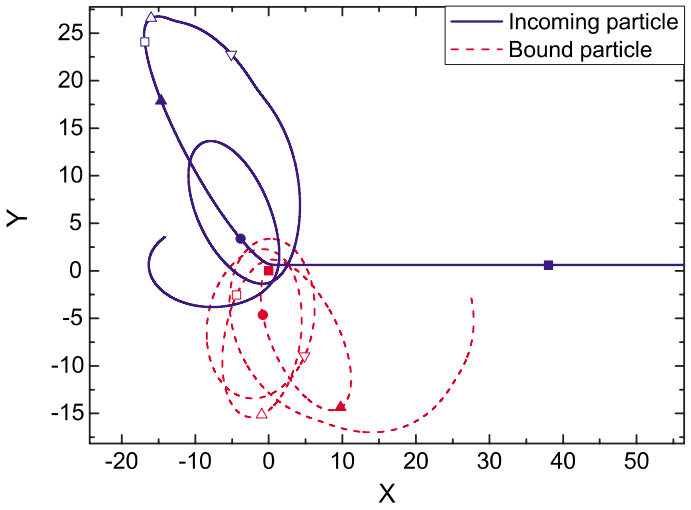

FIG. 11. (Color online) Trajectories for $b=0.6$ and $v=-1.366$. Both particles are close together for a long time (longer than 1000 time units). The symbols indicate the positions of the two particles at different times.

type of collision is observed (the stripe-like pattern). This pattern is also seen in the inset in more detail which may indicate fractal behavior.

We will now characterize this chaotic behavior by calculating the fractal dimension. We call the collection of all initial conditions that lead to a particular type of collision a basin. A point p is a boundary point of a basin B if every open neighborhood of p intersects the basin B and at least one other basin. The set of all these points is called the basin boundary. This boundary is called fractal [13–15] when its box-counting dimension is not integral. This implies in general the existence of an unstable chaotic invariant set embedded in the fractal basin boundary [16].

We will compute the uncertainty dimension of the basin boundaries using the method of Ref. [8]. In a box of initial conditions (b,v), indicated in the inset of Fig. 9, we selected 10^5 random initial conditions. For these initial conditions we calculated the type of scattering. Then we perturbed the initial conditions with a certain ϵ (ϵ from 10^{-4} to 10^{-11}). For these perturbed initial conditions the scattering type was also calculated. When this type was different from the type of the unperturbed conditions, we call the initial condition uncertain. The fraction of uncertain conditions $[f(\epsilon)]$ versus ϵ is then plotted on a log-log scale. According to the theory in Ref. [8] these points should lie on a straight line given by $\log_{10} f = c + \alpha \log_{10} \epsilon$. In this equation the slope α is called the codimension of the basin boundary. The dimension d of the boundary is then found by using $d=D-\alpha$, where D is the dimension of the initial conditions phase space and thus equal to 2. In Fig. 10 we present the result of such a calculation using ten different ensembles, where both b and v were perturbed. The error bars are larger for smaller ϵ values, as the total number of uncertain points becomes smaller. The basin boundary d is equal to 1.41, so clearly fractal (the dimension of a nonfractal boundary is 1). It should be noted that the calculated d is an average of all boundaries appearing in the used box of initial conditions.

An intuitive explanation for the chaotic behavior is given when looking at a typical trajectory in this area. Figure 11 shows that both particles stay close together for a long time. During this time a continuous exchange of energy takes place. The exact trajectories and thus the exact amount of transferred energy depends sensitively on the exact initial conditions. The classification of the collision depends on this exact amount of transferred energy, so it is very hard to predict which type of collision will occur. This can also be seen in Fig. 12 which plots the amount of time that both particles are closer than 30 units of distance of each other, which is a measure of the scattering time. As can be seen this region matches the region where the frequent changes of collision type were detected.

C. High impact parameter asymptotic regime

As can be seen from the scattering regime diagram (Fig. 8) when the impact parameter is larger than 0.9 the incoming particle always scatters to infinity while the initially bound

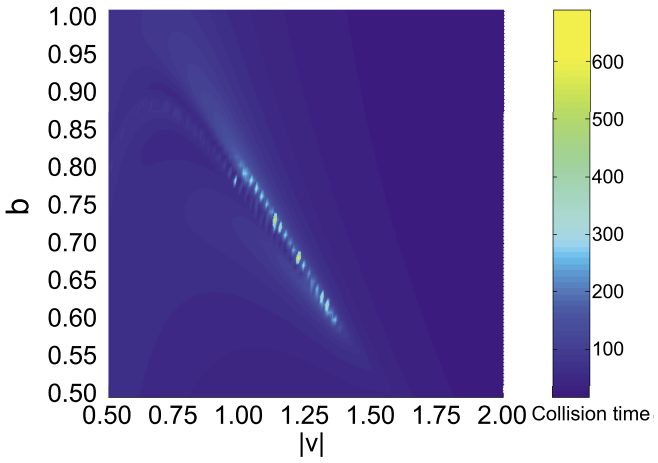

FIG. 12. (Color online) Collision time versus b and v. The area with high collision times coincides with the chaotic region in Fig. 8.

particle remains bound (i.e., scattering of type I). One can expect that when the impact parameter is large enough, i.e., $b \gg 1$, the flyby incoming particle does not disturb substantially the position of the bound one. This reduces the problem to the simple case of scattering on a plane from a central 2D potential of two opposite point charges separated by a distance 1 in reduced units. In the same limit $b \gg 1$ the potential can be approximated with the one of the (properly positioned) electric dipole. Its electric field is axial symmetric, i.e., it has only a radial nonzero component on the plane equal to

$$E_r(r) = \frac{r}{(r^2+1)^{3/2}} - \frac{1}{r^2} \simeq -\frac{3}{2r^4}. \tag{9}$$

The corresponding 2D scattering potential for a negatively charged incoming particle will be

$$V(r) \simeq \frac{1}{2r^3}. \tag{10}$$

Substituting it into Eq. (4) one can express the scattering angle:

$$\theta = \pi - 2\int_{r_m}^{\infty} dr \frac{b/r^2}{[1-(b/r)^2 - 1/(v^2 r^3)]^{1/2}}$$
$$= \pi - 2\int_0^{\xi_m(\alpha)} \frac{d\xi}{[1-\xi^2-\alpha\xi^3]^{1/2}}, \tag{11}$$

with $\xi \equiv b/r$, $\alpha \equiv b^{-3}v^{-2}$, and $\xi_m = b/r_m$ the minimal positive root of the denominator, i.e., of the cubic equation

$$1 - \xi^2 - \alpha\xi^3 = 0. \tag{12}$$

Changing to variable $t \equiv \xi/\xi_m$ the integral in Eq. (11) can be expressed as

$$\theta = \pi - 2\xi_m(\alpha)\int_0^1 \frac{dt}{[1-\xi_m^2 t^2 - \alpha\xi_m^3 t^3]^{1/2}}. \tag{13}$$

Let us introduce a new parameter $g \equiv \alpha\xi_m^3$, which can simplify operations with the integral in Eq. (13). The coefficient of the quadratic term in Eq. (12) then can be expressed as $\xi_m^2 = 1-g$. Note that both α and ξ_m are real and positive implying $0 < g < 1$. We can rewrite the integral in Eq. (13) in the form [21]

$$I_1(g) = \int_0^1 \frac{dt}{\sqrt{(1-t)(1+t+gt^2)}}. \tag{14}$$

The latter can be expressed as the incomplete elliptic integral of the first kind [17].

Equation (12) has only one positive root for all values of α. It can be expressed explicitly using, for example, the Viète's trigonometric formulas (see, e.g., [18]):

$$\xi_m = \frac{2}{3\alpha}\cos\left[\frac{1}{3}\arccos\left(\frac{27}{2}\alpha^2 - 1\right)\right] - \frac{1}{3\alpha}. \tag{15}$$

Together with Eq. (14) and the definition of the parameter g this provides the exact solution for the scattering problem at a central potential Eq. (10) according to Eq. (13).

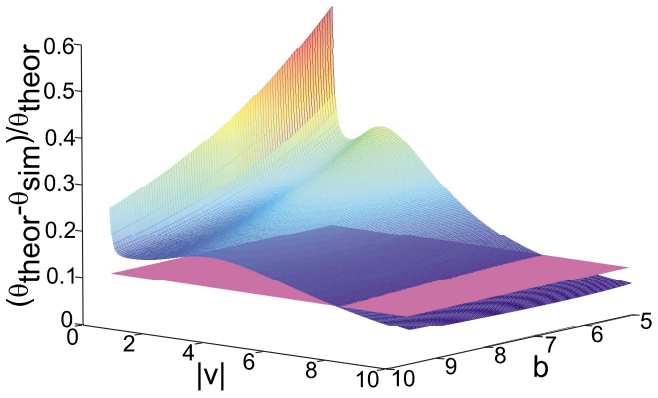

FIG. 13. (Color online) Scattering angle θ versus impact parameter b and initial velocity v in the "flyby" asymptotic limit $b^3v^2 \gg 1$ as compared with the exact numerical result.

Actually, the root $\xi_m(\alpha)$ monotonically decreases from 1 at $\alpha=0$ to 0 at $\alpha \to \infty$. This corresponds to the change of the parameter g in the same limits. The function $I_1(g)$ monotonically decreases on the interval $[0,1]$ from $\pi/2 \approx 1.57$ to $\sqrt{\pi}\Gamma(4/3)\Gamma(5/6) \approx 1.40$. It means that the global behavior of the function $\theta(\alpha)$ is governed mostly by the prefactor $\xi_m(\alpha)$ in Eq. (13).

In the flyby asymptotic regime we can restrict ourselves to the case of small α. In this limit

$$\xi_m \simeq 1 - \frac{\alpha}{2}, \quad g \simeq \alpha, \quad I_1 \simeq \frac{\pi}{2} - \left(1 - \frac{\pi}{4}\right)\alpha. \tag{16}$$

Substituting it into Eq. (13) we finally arrive at the asymptotic expression for the scattering angle:

$$\theta \simeq 2\alpha = \frac{2}{b^3 v^2}. \tag{17}$$

Figure 13 compares the simulation results with this asymptotic dependence. The plane on which the relative difference between the calculation and the simulation is 10% has been drawn to illustrate the fact that the difference becomes smaller in the asymptotic limit.

IV. SUMMARY AND CONCLUSION

We investigated the scattering of a negatively charged particle (an electron) on a classical two-dimensional atomic model system. The Newton equations were numerically integrated by using an adaptive Runge-Kutta algorithm. This model system shows a rich variety of physical phenomena; e.g., it allows one to study different scattering phenomena: elastic scattering, nonelastic scattering, ionization, exchange of particles, and chaos.

We considered two one-particle systems, which were both solved analytically and numerically. Both systems consist of a potential resulting from a positive fixed charge. In the first system the positive charge was located in the same plane as the incoming particle (e.g., Rutherford scattering), while in the other system the positive charge was placed at a distance d from the plane. In both cases the motion of the electron

was constrained to the plane. A qualitative difference was found in the scattering angle as a function of the impact parameter for small b and v. In the limit $b \to 0$ or $v \to 0$, the incoming particle is backscattered in the Rutherford case, while in the other case it is not scattered at all.

When an additional particle is added (corresponding to a classical hydrogen atom) three different types of collisions were identified. The region of appearance of each type was plotted in a scattering regime diagram. A clear distinction could be made between the different cases, except in a small area. In that area the collision type was hard to predict and changed very fast as a function of b or v. It is shown that this area coincides with collisions where both particles stay close together for a long time. This can be understood as an intuitive explanation for the chaotic behavior in this area. It was shown that the basin boundaries have an uncertainty fractal dimension of 1.41. We found that the asymptotic behavior for small b can be fitted to simple equations. In the large b limit it is shown analytically that the system can be described as scattering off a fixed dipole.

ACKNOWLEDGMENTS

This work was supported by the Flemish Science Foundation (FWO-Vl). D.V.T. thanks J.O. Indekeu for interesting discussions.

[1] H. Poincaré, Acta Math. **13**, 1 (1890).
[2] M. Lecar, F. A. Franklin, M. J. Holman, and N. W. Murray, Annu. Rev. Astron. Astrophys. **39**, 581 (2001).
[3] G. A. Farias and F. M. Peeters, Solid State Commun. **100**, 711 (1996).
[4] W. P. Ferreira, A. Matulis, G. A. Farias, and F. M. Peeters, Phys. Rev. E **67**, 046601 (2003).
[5] W. P. Ferreira, F. M. Peeters, and G. A. Farias, Phys. Rev. E **68**, 066405 (2003).
[6] G. Bastard, *Wave Mechanics Applied to Semiconductor Heterostructures* (Les Editions de Physique, Les Ulis, 1988).
[7] T. Ando, A. B. Flower, and F. Stern, Rev. Mod. Phys. **54**, 437 (1982).
[8] E. Ott, *Chaos in Dynamical Systems* (Cambridge University Press, Cambridge, England, 1993), pp. 185–196.
[9] V. Daniels, M. Vallières, and J. Yuan, Chaos **3**, 475 (1993).
[10] E. Ott and T. Tél, Chaos **3**, 417 (1993).
[11] V. A. Schweigert and F. M. Peeters, Phys. Rev. B **51**, 7700 (1995).
[12] G. Sposito, *An Introduction to Classical Dynamics* (Wiley, New York, 1976), pp. 147–153.
[13] C. Grebogi, E. Ott, and J. A. Yorke, Phys. Rev. Lett. **50**, 935 (1983).
[14] C. Grebogi, S. W. McDonald, E. Ott, and J. A. Yorke, Phys. Lett. **99A**, 415 (1983).
[15] S. Takesue and K. Kaneko, Prog. Theor. Phys. **71**, 35 (1983).
[16] C. Grebogi, E. Ott, and J. A. Yorke, Phys. Rev. Lett. **56**, 1011 (1986).
[17] M. Abramowitz and I. A. Stegun, *Handbook of Mathematical Functions* (Dover, New York, 1964).
[18] W. H. Press, B. P. Flannery, S. A. Teukolsky, and W. T. Vetterling, *Numerical Recipes in C: The Art of Scientific Computing* (Cambridge University Press, Cambridge, England, 1992).
[19] This system differs from the one used in classical trajectory Monte Carlo (CTMC) methods, because in this system the electron is initially at rest and the positive core is separated from the plane were the electrons are moving in. Also no random perturbations are used in our approach during the integration of the trajectories. See [20] for a recent study using this technique.
[20] M.-H. Lee, G. Tanner, and N. N. Choi, Phys. Rev. E **71**, 056208 (2005).
[21] S. V. Novikov (private communication).